A fast sensor for non-intrusive measurement of concentration and temperature in turbine exhaust

Rui Zhang[a], Jiangnan Xia[a], Ihab Ahmed[b], Andrew Gough[c], Ian Armstrong[c], Abhishek Upadhyay[a], Yalei Fu[a], Godwin Enemali[a], Michael Lengden[c], Walter Johnstone[c], Paul Wright[d], Krikor Ozanyan[d], Mohamed Pourkashanian[b], Hugh McCann[a], Chang Liu[a,*]

[a] School of Engineering, The University of Edinburgh, Edinburgh, EH9 3JL, UK
[b] Department of Mechanical Engineering, University of Sheffield, Sheffield, S1 3JD, UK
[c] Department of Electronic and Electrical Engineering, University of Strathclyde, Glasgow, G1 1XW, UK
[d] Department of Electrical and Electronic Engineering, The University of Manchester, Manchester, M13 9PL, UK

Abstract

Accurate and rapid measurement of water vapor concentration and temperature in the exhaust of gas turbine engines is critical for monitoring their health and operational performance. To monitor the two parameters simultaneously, a non-intrusive sensor based on tunable diode laser absorption spectroscopy is developed using 8 laser beams targeting 3 transitions of water vapor. The sensor has *in situ* validated on a commercial auxiliary power unit. Seven parallel laser beams at 5000.2 cm^{-1} are 6.3 mm spaced at the plume boundary to characterize the edge effect between hot exhaust plume and cold surrounding flow. One beam, operating at the dual wavenumbers of 7185.6 cm^{-1} and 7444.4 cm^{-1} penetrates the plume through centerline to measure temperature via ratio thermometry and then use this temperature information to obtain the concentration of water vapor. A temporal resolution of 4 milliseconds is achieved for the 8-beam measurement, enabling high-speed and simultaneous quantification of the edge effects and the plume parameters. Results indicate water vapor concentration and temperature in the exhaust measured by the developed sensor are highly consistent with the traditional benchmarks, e.g., extractive sampling and thermocouples, with a difference of 0.02% and 3°C, respectively. Enabled by its continuous millisecond-level measurements, the sensor, for the first time, reveals hidden engine behaviors and combustion dynamics that are unable to be observed by the traditional methods, thus facilitating next-generation real-time gas turbine engine control towards low emissions.

Keywords: TDLAS, gas turbine engine, exhaust plume, water vapor, temperature

1. Introduction

Gas turbine engines (GTEs) are widely used in various industrial sectors including propulsion, power generation and chemical engineering. With the urgent need to achieve carbon neutrality, many improvements in GTE technology are currently underway to allow them to accept fuels that are more environmentally compatible whilst maintaining the safety of GTE operation [1, 2]. The exhaust gas composition and exhaust gas temperature (EGT) are key indicators of GTE combustion efficiency, emissions and health condition [3]. Sustainable aviation fuels (SAFs), for example, are low-carbon alternatives for aviation GTEs, that typically contain a higher ratio of Iso-Paraffins (SIP) and lower ratios of aromatics and cycloparaffin [4]. Therefore, SAFs generally have higher hydrogen content, which results in the generation of high levels of water vapor (H_2O) in the combustion products. Measurements of H_2O becomes increasingly popular for analyzing the chemical reaction using SAFs for GTE [5]. In addition, EGT reflects physicochemical properties relevant to combustion efficiency [6] and more crucially, to predict potential engine failures [7]. Due to the high velocity and turbulent nature of the GTE exhaust plume, as well as the harsh sensing environment, it has been a longstanding challenge for developing *in situ* and robust sensors to monitor H_2O and EGT simultaneously, rapidly, and accurately.

*Email address: c.liu@ed.ac.uk (Chang Liu)

Traditional H_2O and EGT sensors utilizing extractive gas sampling and thermocouples (TCs) suffer from intrusiveness and slow responses. To be specific, H_2O sensors, such as those based on Fourier-transform infrared spectroscopy (FTIR) [8] and gas chromatography [9], require an extractive sampling from the plume to the analytical instruments using heated transportation lines. This system is susceptible to cold spots which results in fluctuation in the measured H_2O concentration level and potentially loss of water due to condensation. Furthermore, gas sampling and analysis introduce sampling residence time, limiting their real-time response when indicating the dynamic changes of the H_2O. Similarly, TCs that are most commonly used for EGT measurement also suffer from slow responses due to their sensing principle based on the heat transfer dynamics and the thermal capacity of the material [10]. Efforts have been directed towards the development of EGT sensors that utilize acoustic and optical modalities to achieve swift measurement capabilities. Acoustic sensors rely on the measurement of temperature-dependent time of flight of sound waves to achieve fast EGT measurement [11]. However, the sound waves are easily perturbed by the high-speed exhaust gas, leading to potential measurement errors. Optical radiation thermometers infer EGT from the heat radiation emitted from reflectors, for example metals, however, they are less quantitative since the measured radiation is contaminated by that in the environment [12].

Tunable diode laser absorption spectroscopy (TDLAS) is a non-intrusive, rapid, and sensitive method for simultaneously measuring H_2O concentration and temperature in reactive flows [13-16]. An early attempt by Liu *et al* demonstrated a line-of-sight (LoS) TDLAS sensor using H_2O transitions and ratio thermometry for EGT measurement on a 20-MW electricity-generating GTE at steady state [17]. Later, Schultz *et al* applied TDLAS techniques to measure the H_2O column density, temperature, and velocity in a modeled scramjet combustor [18]. Both attempts have the emitting and receiving fibers attached to the exhaust chamber casing, which potentially affect the accuracy and precision of the measurements due to the inevitable mechanical vibrations during engine operation. Recently, Upadhyay *et al* introduced a ring-shaped TDLAS tomographic sensor to image the carbon dioxide (CO_2) in the exhaust plume of a large commercial aero-GTE [19]. The non-contact nature of this sensor mitigates the vibrational effects and protects the optical sensor from plume radiation. However, the single CO_2 transition used in the sensor is unable to measure both CO_2 and EGT simultaneously. The measured CO_2 may also suffer from inaccuracy under the assumption of sharp transition of CO_2 concentration from that in ambient air to that in the plume (a 'one-step' model), neglecting the potential existence of a gradient at the plume edge.

To address the above challenges, we designed and implemented an 8-beam TDLAS sensor for *in situ*, simultaneous, accurate and dynamic measurements of both H_2O and EGT. The main novelties of the present paper are summarized as follows:

1. A robust multi-beam TDLAS sensor with 6.3 mm spacing of adjacent beams has been designed to quantify the non-uniform distribution of gas concentration and temperature at the plume edge. The edge compensation technique is then used to correct the LoS TDLAS measurement through the plume centerline. Such sensing capability enables more accurate measurement of both H_2O and EGT at any dynamic GTE working conditions.

2. The developed sensor enables real-time measurement of the physicochemical parameters in the GTE plume with a temporal resolution of 4 milliseconds. Such a fast response reveals the hidden dynamic behaviors of the GTEs that are unable to be observed by the traditional methods.

3. An *in-situ* experiment is carried out to test and validate the developed sensor on a commercial auxiliary power unit (APU). The experimental results agree with the traditional benchmarks at APU steady-state conditions and provide rapid indication of APU control performance at the transient-state conditions.

This paper will commence by introducing the fundamentals of a noise-resistant TDLAS implementation, i.e., wavelength modulation spectroscopy (WMS) with residual amplitude modulation normalization, followed by a discussion on the selection of H_2O transitions for both

ratio-thermometry and plume-edge quantification. It will then detail the sensor design and its validation on the APU in Sections 3 and 4, respectively.

2. TDLAS Measurement Methodology

2.1 Wavelength modulation spectroscopy

WMS is one of the TDLAS implementations that offers strong noise rejection and high sensitivity [20-23]. In this work, we use a driving current of the laser diode that is a superposition of a high-frequency sinusoidal modulation f_m [Hz] with a low-frequency sinusoidal scan f_s [Hz], resulting in modulated laser's output intensity and frequency. The frequency of the modulated laser output, $v(t)$, can be described as:

$$v(t) = \bar{v} + a_s \sin(2\pi f_s t) + a_m \sin(2\pi f_m t), \tag{1}$$

where $\bar{v}$ [cm^{-1}] is the center wavenumber of the laser output spectrum. a_s and a_m are the scan and modulation amplitudes, respectively [24].

Similarly, the laser diode output intensity I_0 can be described as:

$$I_0(t) = \bar{I} + i_s \sin(2\pi f_s t + \varphi_{im}) + i_m \sin(2\pi f_m t + \varphi_{fm}), \tag{2}$$

where $\bar{I}$ is the laser intensity at the center wavenumber $\bar{v}$. i_s and i_m are the amplitudes of the scan and modulation intensites, respectively. φ_{im} and φ_{fm} are the phase differences between the laser intensity modulation and laser frequency modulation, respectively.

When the incident laser beam passes through the target absorbing gas species and is received by a photodetector, the transmitted laser intensity I_t can be described using the Beer-Lambert law:

$$I_t(t) = I_0(t)\exp[-A\phi(v(t), T, P, \chi)]. \tag{3}$$

where ϕ is the lineshape of the spectral absorption feature, which is a function of $v(t)$, temperature T [K], the total pressure of the absorbing species P [atm], and gas mole fraction χ. A is the path-integrated absorption:

$$A = \int_0^L S(T) P \chi \, dl, \tag{4}$$

where $S(T)$ [cm^{-2}atm^{-1}] is the temperature-dependent line strength and L [cm] is the absorbing path length.

In the WMS technique, the interaction of $v(t)$ and $I_0(t)$ described in (1) and (2) with the absorbing gas results in the generation of signals that can be described as a Fourier series of terms at the harmonics of the high frequency sinusoidal modulation. Using lock-in amplification to recover the first- and second-order harmonics of I_t, denoted 1f and 2f, allows the use of a calibration-free WMS technique [24, 25]. The technique normalizes the 2f spectrum by the 1f spectrum, denoted as WMS-2f/1f:

$$\text{WMS-}2f/1f = \sqrt{\left[\left(\frac{X_{2f}}{R_{1f}}\right)_{raw} - \left(\frac{X_{2f}}{R_{1f}}\right)_{bg}\right]^2 + \left[\left(\frac{Y_{2f}}{R_{1f}}\right)_{raw} - \left(\frac{Y_{2f}}{R_{1f}}\right)_{bg}\right]^2}, \tag{5}$$

where X_{nf} and Y_{nf} (n = 1 or 2 here) denote the in-phase and quadrature components of the n^{th} harmonics. $R_{nf} = \sqrt{X_{nf}^2 + Y_{nf}^2}$ is the magnitude of the n^{th} harmonic. $(.)_{raw}$ and $(.)_{bg}$ denote signals obtained with and without absorption, respectively. The measured WMS-2f/1f signal can be least square fitted to a simulated spectrum using the Voigt line-shape function and the HITRAN database [26]. As a result, A in (4) can be extracted from the fitting results. Two path-integrated absorption values, A_1 and A_2, can be obtained by fitting two spectral features of the same gas species, and their ratio, $R(T)$, is used to calculate the temperature along the light path as follows:

$$R(T) = \frac{S_2(T)\chi L}{S_1(T)\chi L} = \frac{S_2(T)}{S_1(T)}, \tag{6}$$

where the parameters with subscripts 1 and 2 refer to the two spectral features that have been selected with different dependencies of linestrength on temperature. This method is known as ratio thermometry [15, 22]. With T in hand, χ can be calculated using either of the two transitions according to (4).

2.2 Line selection

Table 1 shows the spectral parameters of the three H_2O absorption lines utilized by the sensor described here. Their central wavenumbers are $\bar{\nu}_1$ = 5000.2 cm^{-1}, $\bar{\nu}_2$ = 7185.6 cm^{-1} and $\bar{\nu}_3$ = 7444.4 cm^{-1}. Figure 1 illustrates H_2O absorbance spectra at room temperature, 21°C, and typical EGT, 400°C, when L = 50 cm, P = 1 atm and typical H_2O molar fraction in the exhaust as 5 %, with black and red curves, respectively. At EGT-similar temperatures, all primary absorption lines provide 0.2 and above peak absorbance, enabling good signal to noise ratio (SNR) of the measured WMS-2*f*/1*f*.

The absorption feature at $\bar{\nu}_1$ (t1 in Table 1) is composed of a single spectral transition. In the sensor designed here, $\bar{\nu}_1$ is utilized to characterize the non-uniformity at the plume edge as the probability of absorption at room temperature is more than 50 times lower than the assumed absorption of the plume, therefore ensuring minimal optical absorption due to ambient H_2O outside the plume. In addition, $\bar{\nu}_1$ falls in a frequency range where the optical power can be amplified using a thulium-doped fiber amplifier (TDFA) [19]. This allows use in a multi-channel sensor system whilst ensuring the optical power on each detector is maximized to provide the highest SNR, as described in section 3.

The absorption features at $\bar{\nu}_2$ and $\bar{\nu}_3$ are used for temperature and H_2O concentration measurement. These features have been widely used in ratio thermometry with proven sensitivity in the temperature range of 21°C to 800°C [27, 28], which covers the EGT range at different engine loads. $\bar{\nu}_2$ is comprised of two adjacent transitions (t2, t3 in Table 1) with a stronger absorption at

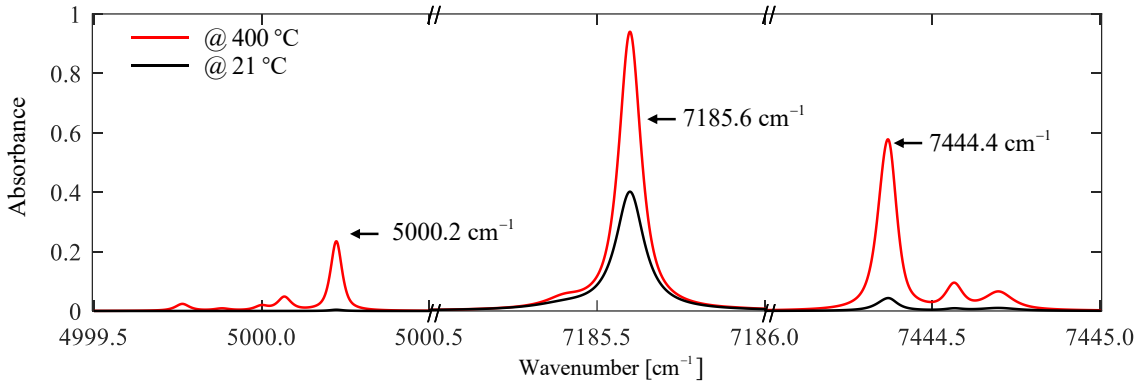

Figure 1: Absorbance spectra at 21°C and 400°C for the selected H_2O lines assuming L = 50 cm, χ = 5 % and P = 1 atm.

Table 1: Spectral parameters of the selected H_2O lines at P = 1 atm (HITRAN database)

Spectral lines / Parameters	$\bar{\nu}_1$	$\bar{\nu}_2$		$\bar{\nu}_3$		
	t1	t2	t3	t4	t5	t6
$\bar{\nu}$ (cm^{-1})	5000.223	7185.596	7185.597	7444.351	7444.368	7444.371
S (cm^{-2}atm^{-1}) at T= 21°C	5.842×10^{-5}	4.819×10^{-3}	1.446×10^{-2}	5.187×10^{-4}	1.475×10^{-4}	4.428×10^{-4}
S (cm^{-2}atm^{-1}) at T= 400°C	5.124×10^{-3}	1.033×10^{-2}	3.098×10^{-2}	8.742×10^{-3}	2.721×10^{-3}	8.168×10^{-3}
E'' (cm^{-1})	2358.302	1045.058	1045.057	1774.750	1806.670	1806.669
HWHM (cm^{-1})	0.0323	0.0655	0.0711	0.0523	0.0503	0.0467

ambient temperature, while $\bar{\nu}_3$ is a high-temperature feature comprising of three adjacent transitions (t4, t5, t6 in Table 1).

3. Sensor design

The schematic diagram of the sensing system is shown in Figure 2, which consists of laser driving, optical distribution, optical detection, and data acquisition (DAQ).

The optical signals at $\bar{\nu}_1$, $\bar{\nu}_2$ and $\bar{\nu}_3$ are generated by three distributed-feedback (DFB) laser diodes, Nanoplus 2000 nm DFB, NEL NLK1E5EAAA and NEL NLK1B5EAAA, respectively. Each DFB laser diode is temperature- and current-controlled by a laser driver (Wavelength Electronics, LDTC 2-2E). Temperature control is used to ensure the central wavenumber of each laser output is maintained. The frequencies of driving currents for the three lasers are shown in Table 2. All three lasers are scanned with f_s = 1 kHz sinusoidal wave. Signal generator 1 controls the injected current waveform to scan across 5000.2 cm^{-1} with a 130 kHz high-frequency modulation. The two lasers at 7185.6 cm^{-1} and 7444.4 cm^{-1} are frequency division multiplexed (FDM) to simultaneously measure the gas properties within the same gas medium [28]. Compared with the time division multiplexing (TDM) [29, 30], FDM is more suitable for measure gaseous targets with high dynamics, where penetrating temporal response is needed to resolve the rapid change of gas properties. Signal generator 2 provides different modulation frequencies to the two laser controllers at 100 kHz and 130 kHz. The 30kHz separation of the modulation avoids frequency aliasing on the 1f and 2f signals.

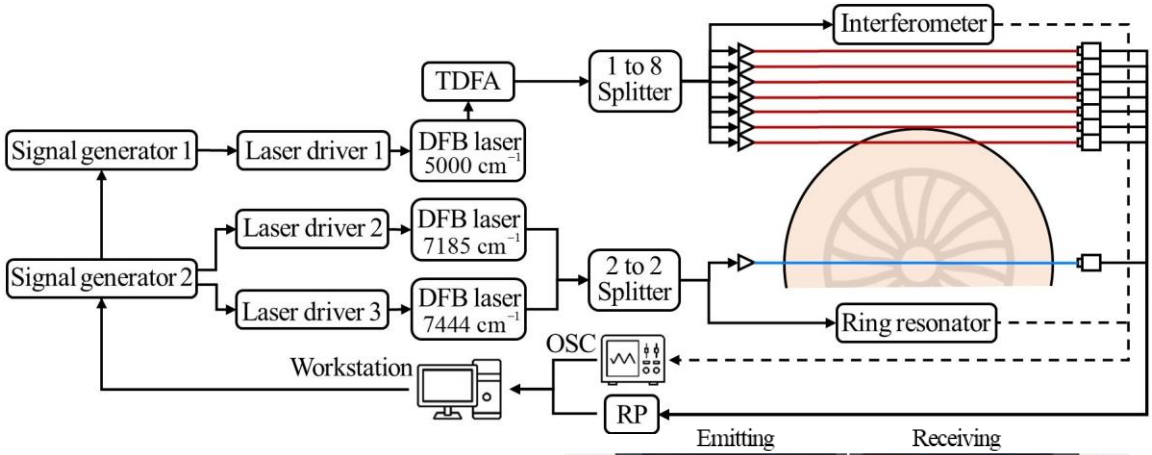

Figure 2: Schematic diagram the developed sensing system.

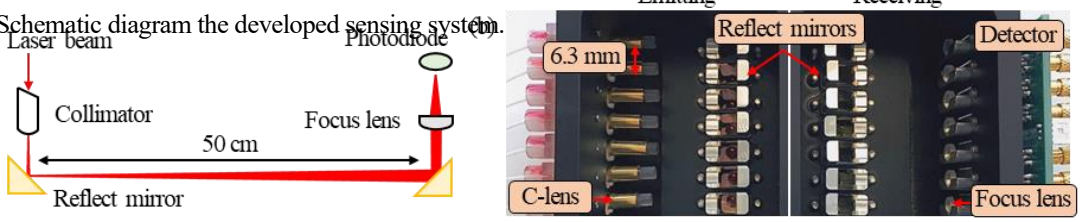

Figure 3: Optical layout of (a) a single laser-beam measurement and (b) 7 laser beams located at the plume edge.

Table 2: Laser driving parameters of the three tunable laser diodes used in the sensor

$\bar{\nu}$ (cm^{-1})	Sinusoidal scan frequency f_s [Hz]	Sinusoidal modulation frequency f_m [Hz]	Coupling	DAQ
5000.2	1 kHz	130 kHz	1x8	7 detected by RP @ 15.625 MSps 1 detected by OSC @ 500 MSps
7185.6	1 kHz	100 kHz	2x2	1 detected by RP @ 15.625 MSps
7444.4		130 kHz		1 detected by OSC @ 500 MSps

Since the power of the laser diode at 5000.2 cm^{-1} is less than 2 mW, the output laser is amplified by a TDFA (Keopsys) and then equally split into eight beams using a 1-to-8 fused fiber splitter. As shown in Figure 2, seven of the eight beams are equally and closely spaced, with 6.3 mm spacing, to characterize the plume edge, whilst the eighth is passed through a Mach–Zehnder interferometer with free spectra range (FSR) as 0.06 cm^{-1} for $v(t)$ characterization. The optical signals from the lasers at 7185.6 cm^{-1} and 7444.4 cm^{-1} are combined and then split into 2 beams using a 50:50 fiber coupler. One of the two coupler outputs penetrates the plume center to measure H_2O concentration and temperature, while the other is used for $v(t)$ characterization through a ring resonator with FSR as 0.0107 cm^{-1}.

The optics design for each laser-beam measurement is shown in Figure 3(a). The optical beams are emitted using C-lens collimators. Two 5 mm gold-coated prism mirrors enable adjustment of beam direction on both emitting and receiving ends. The transmitted laser beam is then focused by a 4 mm plano-convex lens. Considering a very small beam spacing is required in this design, small photodiodes (Hamamatsu, G12182-010K) are placed at the focus of the plano-convex lens. When the space at the receiving end is not limited, quartz crystal tuning fork could also be a detection option for FDM of multiple lasers [31]. After traversing a 50 cm light path, the laser spot is ~2 mm in diameter, which underfills the photosensitive target after being focused by the plano-convex lens. A single-ended transimpedance amplifier was designed based on a low-noise AD8066 operational amplifier, converting the photodiode current output to a voltage signal with an amplification factor of 1k and a -3 dB bandwidth of 6 MHz. Such a high bandwidth guarantees no signal attenuation on the laser transmission and their harmonics. Both the emitting and receiving opto-mechanics are enclosed by aluminum cases with small apertures, protecting the sensor from heat radiation and turbulent disturbance. Figure 3(b) shows the assembly of the 7 laser beams located at the plume edge. Since the diameter of the photodiode's TO-18 cap is 5.6 mm, the minimum manufacturing tolerance allows a beam spacing of 6.3 mm while maintaining 5°angular adjustment freedom. As detailed in section 4, the small beam spacing enabled by our design greatly improves the spatial resolution for compensating the non-uniformity of the gas parameters at the plume edge, thus leading to more accurate retrieval of the H_2O and EGT.

All sensing signals are digitized by a Red Pitaya (RP)-based DAQ system [32]. A signal conditioning circuit (SCC) is designed to amplify and multiplex the laser transmissions to be digitized by the RP. The SCC consists of four dual-channel programmable gain amplifiers (THS7002, Texas Instruments) and two 4-to-1 multiplexers (ADG704, analog devices), which are digitally controlled by the FPGA I/Os on the RP. To be specific, the programmable gain amplifiers condition the raw signals to 0-1 V, that is, within the input range of the analogs to digital converters (ADCs) on the RP. Then, the multiplexers are used for fast TDM across every 4-channel signal at the intervals of consecutive periods of the wavenumber scan, giving a final time resolution of 250 Hz for each of the 4 optical beams. The multiplexed signal is collected by the ADCs on the RP. RP offers a maximum of 125 Mega Samples/second (MSps) sampling rate of each ADC. It is much excessive to sample the laser transmissions and their harmonics, i.e., 1f signals at 100 kHz and 130 kHz, 2f signals at 200 kHz and 260 kHz, of the developed sensor. To reduce data streaming rate and the amount of data to be stored, decimation at the hardware level was implemented. We averaged the adjacent points to achieve a decimation rate of 8. Then, the sampling rate becomes 15.625 MSps. The inputs to the RP are demodulated using the integrated FPGA on the RP to obtain the 1f and 2f spectra, which are then transferred to the workstation via Ethernet.

4. Experimental Section

4.1 APU

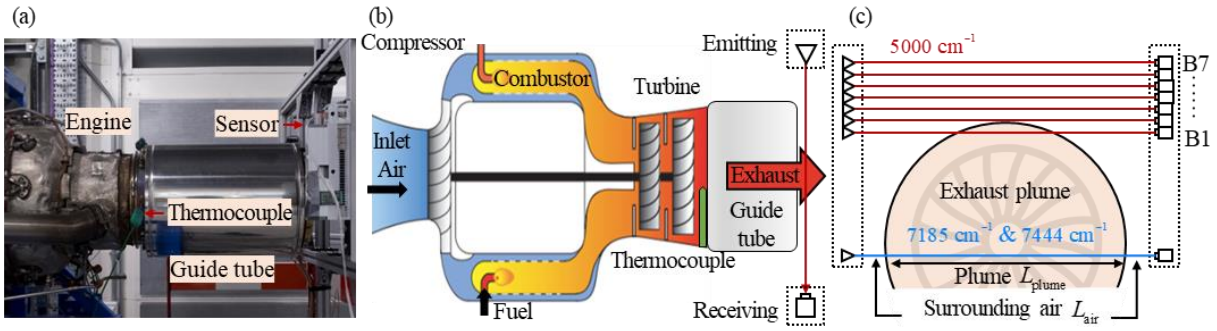

Figure 4: *In situ* experimental system. (a) and (b) show the picture and the schematic layout of the APU and the sensor. (c) shows the optical layout at the APU exit.

In situ validation of the developed sensor is performed on a commercial APU (Honeywell 131-9A). Figure 4 illustrates the APU and the positioning of the developed sensor relative to the APU exhaust plume. A guide tube with a length of 30 cm and a diameter of 25 cm is attached to the rear of the APU exit, to direct the flow into the exhaust system. The laser sensor is mounted on a plane 3 cm downstream of the outlet of the guide tube. A K-type TC is inserted at the inlet of the guide tube as shown in Figure 4(b), providing a reference EGT during the test. As the APU exhaust velocity is up to 100 m/s, the temperature difference at the inlet and outlet of the guide tube is assumed to be negligible.

4.2 Non-uniformity characterization

When the APU is operating, the hot exhaust plume mixes with cold ambient air at the guide tube outlet, resulting in non-uniform radial profiles of H_2O and EGT along the plume edge. Failing to consider for this non-uniformity will cause systematic errors in TDLAS recovery of EGT and χ [33]. A FTIR extractive gas sampling probe and a K-type TC, shown in Figure 5(a), were scanned horizontally across the center of the plume on the same plane as the laser measurement during APU steady full-load operation to measure the non-uniformity of the plume-edge. The pointwise measurements of H_2O and EGT along the scan are shown in Figure 5(b) by the black and red dashed lines, respectively, showing trapezoidal radial profiles for both measurements. The H_2O and EGT at the plateau are 3.6 % and 490 °C respectively. They decrease rapidly beyond the diameter of the guide tube outlet. In principle, the plume is rotationally symmetric at the steady state. The asymmetry between rising and falling edge of the temperature profile shown in Figure 5(b) is assumed to be due to the inherited lag of the TC measurement, since the heat is aggregated on the TC during the scan. It is also worth noting that the profiles measured by the extractive gas sampling and TC are only valid when the APU is operating under steady-state conditions. They are not valid during APU startup, in which the dynamic process cannot be captured by the slow mechanical scan.

Assuming rotational symmetry of the χ and EGT distributions, the above non-uniformity can also be measured at 250 Hz using the 7 optical signals located around the plume edge, shown in Figure 4(c), with beam B2 aligned with the edge of the guide tube outlet. Figure 5(c) shows typical $2f/1f$ signals at 5000.2 cm^{-1} under steady full-load condition, with their peak-values marked by asterisks that are assumed to indicate the magnitude of the path-integrated absorption. Figure 5 shows that the $2f/1f$ magnitudes gradually decrease from B1 to B3, indicating the decreasing absorption around the plume edge. The normalized χ, T and asterisked values for B1-B7 are plotted in Figure 5(d). The indicated gradient from B1-B3 on the plume edge agree well with that obtained from the extractive gas sampling and TC measurements. In addition, B4-B7 consistently show very weak absorption, indicating they are measuring predominantly ambient air. For real-time analysis, the edge effect is quantified simultaneously with the gas measurement in the plume at 250 Hz, enabling accurate measurement of both H_2O and EGT at any dynamic GTE working conditions.

The above radial information can be used to characterize the absorption along the beam that traverses the center of the plume, with path length in the hot plume L_{plume} including the non-uniform plume-edge effects, whilst also defining the length of the beam-path in the ambient air L_{air}. From the TDLAS radial profile measurements at steady full-load condition, as shown in Figures 5(c-d), we define the plume radius to extend out to the radial position of B4, giving L_{plume} = 275.2 mm and L_{air} = 224.8 mm. The H_2O molar fraction and EGT, denoted χ_{plume}, and T_{plume}, respectively along the whole path length in the plume can be calculated by:

$$S(T_{plume})\chi_{plume}PL_{plume} = S(T_{meas})\chi_{meas}PL_{meas} - S(T_{air})\chi_{air}PL_{air}, \quad (7)$$

where $(.)_{plume}$ and $(.)_{air}$ denote the gas parameters in the plume and in the air, respectively. Here, χ_{air} = 0.6 % and T_{air} = 24.5 °C were measured independently in the APU test cell. In the analysis below, the TDLAS measurements of χ_{plume} and T_{plume} are those obtained from (7).

To facilitate the comparison between the above TDLAS measurements and those provided by the benchmark extractive gas sampling and the TC, we calculate the TDLAS path-integrated absorption that would be expected, for each spectral absorption feature at $\bar{v}_2$ and $\bar{v}_3$ in the HITRAN model, by applying the H_2O and EGT scanned measurements over the path length L_{plume} as defined above. Consequently, the equivalent temperature along light path, T_{eq}, can be obtained by ratio thermometry as follows:

$$R(T_{eq}) = \frac{\sum_L S_2(T_j)P\chi_j l_j}{\sum_L S_1(T_j)P\chi_j l_j}, \quad (8)$$

where χ_j and T_j denote the H_2O concentration and temperature in j^{th} discretized path length l_j = 6.3 mm along the scan. Then, the equivalent H_2O concentration, χ_{eq}, is calculated by (4) using either of the two transitions. The black and red solid lines in Figure 5(b) shows χ_{eq} and T_{eq} calculated from the non-uniform profiles. χ_{eq} and T_{eq} are, respectively, 0.2% and 50°C below the

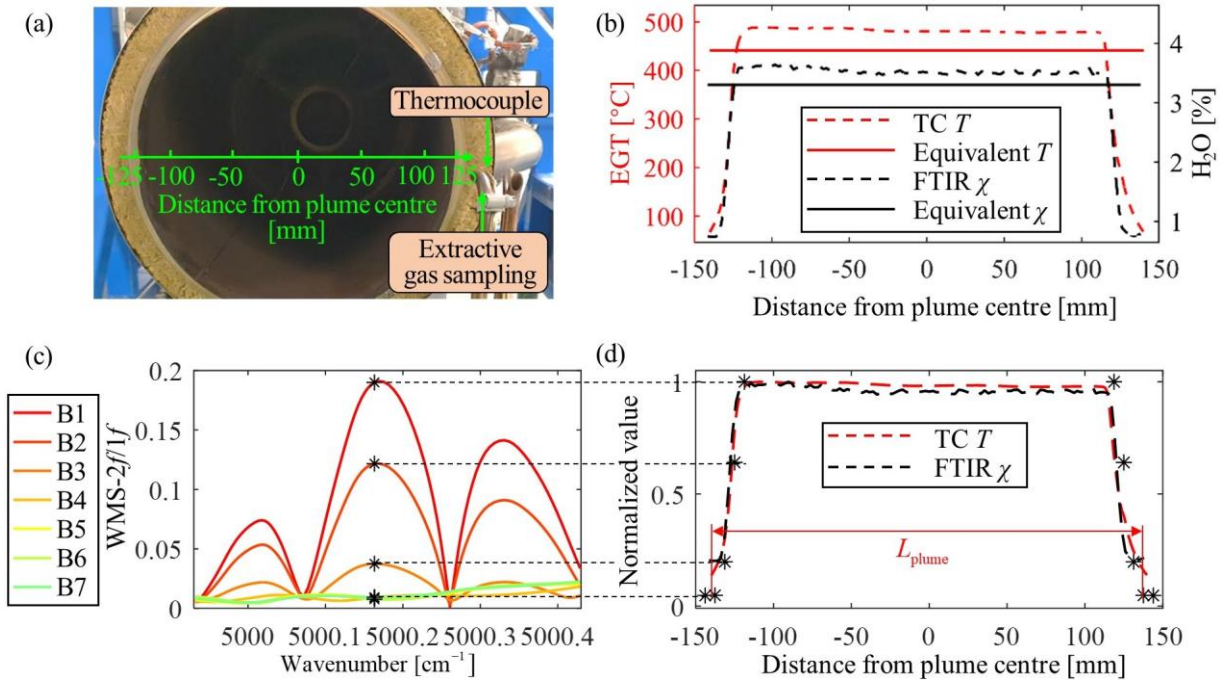

Figure 5: Non-uniformity characterization at APU plume edge using scanned extractive gas sampling and TC, and the developed TDLAS sensor. (a) shows the path of the mechanical scan using the benchmarks methods at the exit of the APU. (b) shows pointwise measurement of temperature and H_2O concentration along the scan and their TDLAS-equivalent values under steady full-load conditions, and the equivalent values for the whole plume path length calculated via HITRAN (see text). (c) shows WMS-2*f*/1*f* obtained for each of the 7 beams at the plume edge. (d) shows the comparison between the non-uniform profile retrieved using the TDLAS sensor and benchmarks.

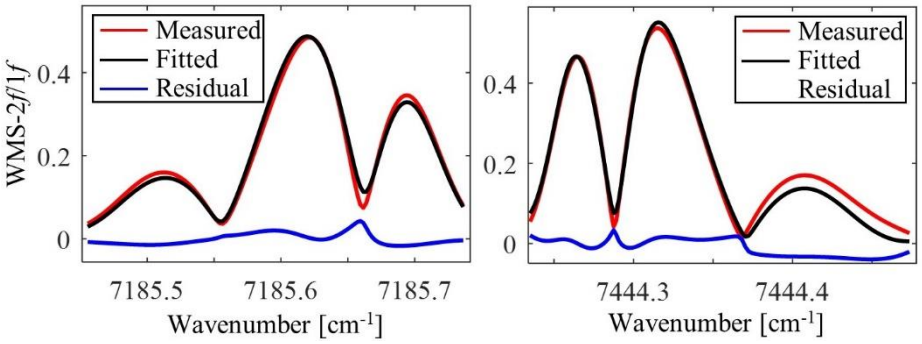

Figure 6: An example of measured and fitted WMS-2f/1f signal at 7185 $cm^{-1}$and 7444 cm^{-1} when applying the developed TDLAS sensor to the APU exhaust monitoring.

Table 3: *In situ* measured H_2O and EGT at the APU full-load condition

	TDLAS H_2O (%)	Reference H_2O (%)	TDLAS EGT (°C)	Reference EGT (°C)
Mean	3.38	3.40	442.13	439.15
STD	4.5×10^{-3}	2.6×10^{-3}	9.65	3.57

extractive gas sampling and TC measurements at the plateau, respectively.

A separate test was carried out to validate the above characterization when the APU is stabilized at the full-load condition. Table 3 shows the mean and variance of H_2O and EGT measured over 120 seconds during the full-load operation, generating 30,000 samples for the TDLAS and 1,200 samples for the FTIR (10 Hz) and TC (10 Hz). One example of fitting of the WMS-2*f*/1*f* signal at this stage is shown in Figure 6. Overall, the mean values of H_2O and EGT obtained using the TDLAS agree very well with the benchmarks, with a difference of only 0.02 % and 3°C, respectively, demonstrating good accuracy of the developed sensor. In addition, the TDLAS measurements show excellent precision, with standard deviation (STD) of mean values of 4.5×10^{-3} % in H_2O and 9.65°C in EGT. The slightly larger values of STD observed in TDLAS measurements of H_2O and EGT compared to those obtained using the gas sampler and TC are likely to be caused by their different temporal responses, i.e., the variations introduced by the plume turbulence are more likely to be smoothed out by the slow-response benchmarks, captured at a slower sampling rate.

4.3 Dynamics analysis

In this experiment, H_2O, χ_{plume}, and EGT, T_{plume}, were measured dynamically using the developed sensor from APU start-up to the steady-state conditions in a period of 120 seconds. The APU was controlled by an engine control unit (ECU) and went through four operating conditions: ignition, acceleration, no load, and pneumatical full load. Figure 7 shows the comparison between the H_2O (black solid line) and EGT (red solid line) measured by TDLAS at 250 Hz, and the equivalent EGT based on the measurement of TC (red dashed line) at 10 Hz. The time axis is synchronized by the turbine speed sampled at 10 Hz (black dashed line). The TDLAS EGT measurements match the reference EGT very closely at the two steady states, i.e., the no load and pneumatical full load conditions. In the following, we further analyze the dynamic measurement results under each APU operating condition.

4.3.1 Ignition and Acceleration

Figure 8(a) shows the transient states recorded from engine start up for a period of 40 seconds. From time, t = 0 to 6 s, the motor provides initial power to spin the turbine, enabling air to flow through and mix with the Jet-A1 fuel prior to ignition. When the turbine speed reaches about 5×10^4 rpm, the fuel-air mixture is ignited. At this point, the H_2O and EGT

increase rapidly in the exhaust plume, peaking at 6.74 % and 517.5 °C, respectively. Following ignition, from t = 6 to 40 s, the fuel flow rate is increased to steadily accelerate the turbine until the APU passes the point of no return (PNR) at t = 10 s. During this process, the ECU dynamically controls the fuel injection to prevent excessive EGT that can potentially damage the engine. Beyond the PNR, the APU becomes self-sustained. Then the turbine speed can be increased with decreased fuel consumption, resulting in reduction of H_2O and EGT from their peak values. Overall, the profile of H_2O measured using the TDLAS sensor exhibits strong correlation with the temperature profile. A more significant gap between the two can be observed after t = 15s. Then, EGT is steady while H_2O falls due to the decreased fuel injection.

The high temporal resolution of the TDLAS sensor reveals at least three APU behaviors not observable using the traditional extractive sampling and TC methods during this period: Firstly, the TDLAS measurements accurately indicate the successful ignition of the APU with

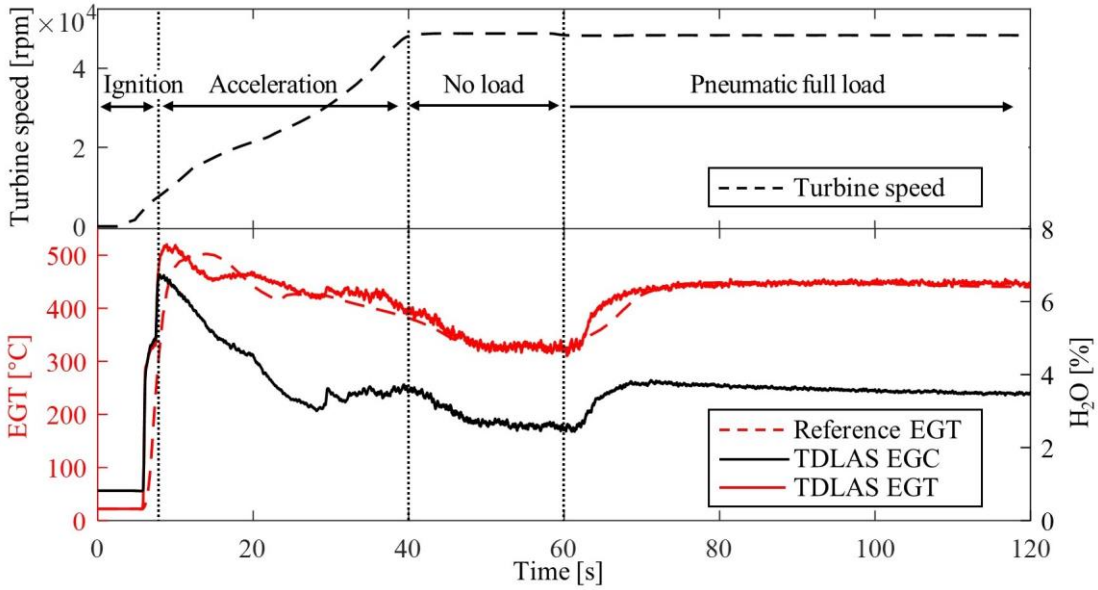

Figure 7: Comparison of dynamic H_2O and EGT obtained using the developed sensor and the TC under varying turbine speed for a 120-second APU experiment.

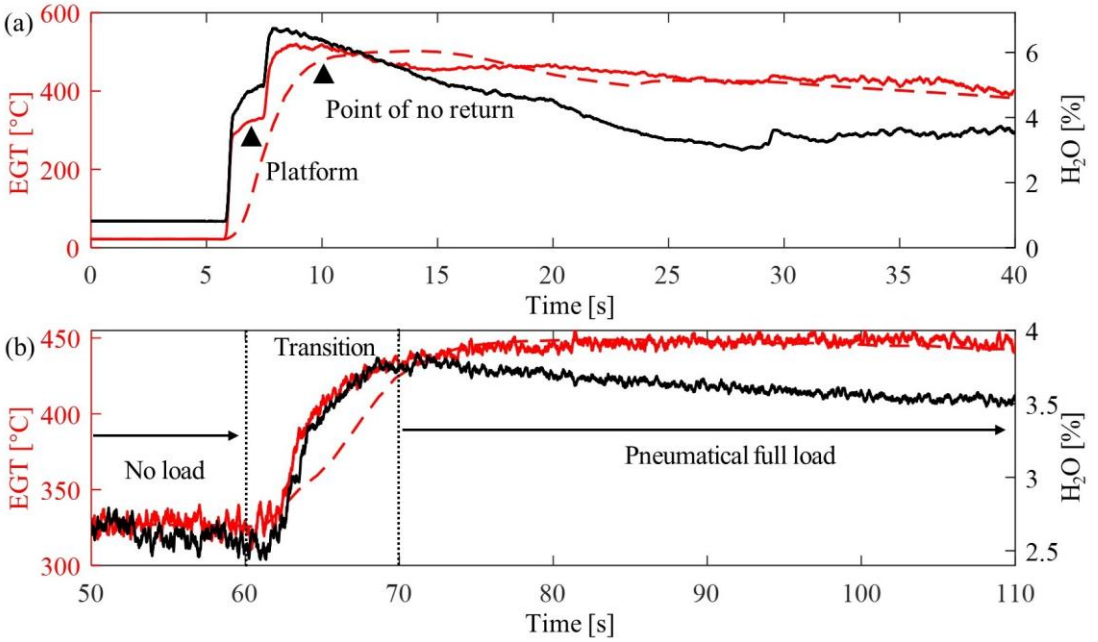

Figure 8: Dynamically sampled H_2O and EGT using the developed sensor under different APU operating conditions, i.e., (a) transient states for ignition and acceleration; (b) The transition period from no-load to the full-load steady-state condition.

abrupt increase in H_2O and EGT at t = 6 s shown in Figure 7(a) above, while the TC only shows a delayed, smooth EGT increment. Secondly, the TDLAS measurements resolve a temporary platform between (7-8 s). This platform is missing in TC measurements due to slow temporal response. Finally, the TDLAS sensor reveals a higher and earlier peak EGT. Its rapidness could facilitate further improvement of the state-of-the-art mode of fuel injection.

4.3.2 No load and full load

After reaching the required turbine speed of 4.9×10^4 rpm, the APU enters a steady no load working condition from 40 to 60 s. Within this period, the H_2O and EGT measured by the TDLAS sensor are stabilized at around 2.46 % and 330 °C respectively. From 60 s, the APU starts to be loaded by controlling the bleed air flow. The inlet guide vanes between the compressor and the air inlet are opened to match the demand compressor flow. More fuel is injected to maintain the turbine speed at 4.8×10^4 rpm. The transition between conditions and the fuel flow is smooth and steadily controlled by the ECU. In Figure 8(b), both the H_2O and EGT increase rapidly between 60 s and 70 s before settling to 3.71% and 445.5 °C in the steady-state of full load, respectively. Similar to the condition of acceleration, a decreasing tendency can be observed for the H_2O since less fuel is needed once the turbine speed can be maintained at full load condition.

It is worth noting that the plume edge compensation approach, validated for one static condition in subsection 4.2, has been used in the no load and full load static conditions, where no radial reference of H_2O and EGT were taken. The stabilized EGT 50-60 s and 75-110 s in Figure 7 obtained by the TDLAS sensor also agree very well with the TC measurement. This indicates good accuracy of the plume edge compensation technique for measuring varying physicochemical parameters in the highly turbulent APU exhaust.

The TDLAS measurements show transient responses consistent with increment in the fuel injection rate. According to Figure 8(b), the step responses of H_2O and EGT can be modelled as

$$\Delta\chi(t) = 1.21\times(1-e^{-t/2.22}), \tag{9}$$

$$\Delta T(t) = 109.38\times(1-e^{-t/3.21}), \tag{10}$$

where the $\Delta\chi$ and ΔT denote the responses of H_2O and EGT on the fuel injection.

However, the above step responses cannot be revealed using the TC. As shown in Figure 8(b), the EGT obtained using the TC in the transition period shows a more linear performance, which disagrees with the nature of the step increment of fuel injection. Therefore, it can be concluded that the high-speed TDLAS sensor working is superior to the benchmark, i.e., extractive gas sampling and TC, in terms of more accurate measurement of the dynamics of turbulent exhaust.

5. Conclusions

This paper describes the development and testing of a multi-channel TDLAS sensor for simultaneous and rapid monitoring of H_2O and EGT of GTEs. Seven beams emitted by a DFB laser working at 5000.2 cm^{-1} reveal the trapezoidal absorption distribution at the plume edge with a spatial resolution of 6.3 mm. Two frequency division multiplexed lasers working at 7185.6 cm^{-1} and 7444.4 cm^{-1} exploit the H_2O absorption line pair for H_2O and EGT measurements. The sensor was validated by performing extractive gas sampling and TC measurements on a commercial APU. The developed sensor exhibited good accuracy during the APU steady-stage condition, demonstrating a 0.02% molar fraction and a 3°C temperature difference with those obtained by benchmarks, i.e., extractive gas sampling and thermocouple. The sensor has much better temporal resolution (4 ms) than the intrusive measurements, which has provided additional insight into underlying GTE dynamic behaviors, viz. H_2O and EGT variation during engine ignition and

subsequent fuel injection increase.

Acknowledgement

The authors would like to acknowledge the financial support from EPSRC Programme Grant LITECS (EP/T012595/1).

Reference

[1] Y. Liu, X. Sun, V. Sethi, D. Nalianda, Y.-G. Li, and L. Wang, "Review of modern low emissions combustion technologies for aero gas turbine engines," *Progress in Aerospace Sciences,* vol. 94, pp. 12-45, 2017.

[2] D. Burnes and A. Camou, "Impact of fuel composition on gas turbine engine performance," *Journal of Engineering for Gas Turbines and Power,* vol. 141, no. 10, p. 101006, 2019.

[3] U. Ahmed, F. Ali, and I. Jennions, "A review of aircraft auxiliary power unit faults, diagnostics and acoustic measurements," *Progress in Aerospace Sciences,* vol. 124, p. 100721, 2021.

[4] K. S. Ng, D. Farooq, and A. Yang, "Global biorenewable development strategies for sustainable aviation fuel production," *Renewable and Sustainable Energy Reviews,* vol. 150, p. 111502, 2021.

[5] W. Zhang, D. J. Webb, L. Lao, D. Hammond, M. Carpenter, and C. Williams, "Water content detection in aviation fuel by using PMMA based optical fiber grating," *Sensors and Actuators B: Chemical,* vol. 282, pp. 774-779, 2019.

[6] S. Manigandan, A. Atabani, V. K. Ponnusamy, and P. Gunasekar, "Impact of additives in Jet-A fuel blends on combustion, emission and exergetic analysis using a micro-gas turbine engine," *Fuel,* vol. 276, p. 118104, 2020.

[7] L. Liu, Q. Guo, L. Wang, and D. Liu, "In-situ remaining useful life prediction of aircraft auxiliary power unit based on quantitative analysis of on-wing sensing data," *Advances in Mechanical Engineering,* vol. 12, no. 3, pp. 1-13, 2020.

[8] B. Giechaskiel and M. Clairotte, "Fourier transform infrared (FTIR) spectroscopy for measurements of vehicle exhaust emissions: A review," *Applied Sciences,* vol. 11, no. 16, p. 7416, 2021.

[9] A. Rafoth, S. Gabriel, F. Sacher, and H.-J. Brauch, "Analysis of isothiazolinones in environmental waters by gas chromatography–mass spectrometry," *Journal of Chromatography A,* vol. 1164, no. 1-2, pp. 74-81, 2007.

[10] B. George and N. Muthuveerappan, "Life assessment of a high temperature probe designed for performance evaluation and health monitoring of an aero gas turbine engine," *International journal of turbo & jet-engines,* vol. 40, no. 2, pp. 139-146, 2020.

[11] R. Otero Jr, K. T. Lowe, W. F. Ng, L. Ma, and C.-Y. Kim, "Nonintrusive gas-turbine engine-exhaust characterization using acoustic measurements," *Journal of Propulsion and Power,* vol. 34, no. 3, pp. 730-738, 2018.

[12] D. H. Shin, M. Kim, J. S. Kim, B. J. Lee, and J. Lee, "Precise infrared thermometry with considering background radiation for gas turbine air cooling application," *International Journal of Thermal Sciences,* vol. 158, p. 106534, 2020.

[13] J. Li, H. Deng, J. Sun, B. Yu, and H. Fischer, "Simultaneous atmospheric CO, N2O and H2O detection using a single quantum cascade laser sensor based on dual-spectroscopy techniques," *Sensors and Actuators B: Chemical,* vol. 231, pp. 723-732, 2016.

[14] J. Li *et al.*, "In situ, portable and robust laser sensor for simultaneous measurement of ammonia, water vapor and temperature in denitrification processes of coal fired power plants," *Sensors and Actuators B: Chemical,* vol. 305, p. 127533, 2020.

[15] W. Wang, Z. Wang, and X. Chao, "Gaussian process regression for direct laser absorption spectroscopy in complex combustion environments," *Optics Express,* vol. 29, no. 12, pp. 17926-17939, 2021.

[16] Z. Qu, P. Holmgren, N. Skoglund, D. R. Wagner, M. Broström, and F. M. Schmidt, "Distribution of temperature, H2O and atomic potassium during entrained flow biomass

combustion–Coupling in situ TDLAS with modeling approaches and ash chemistry," *Combustion and Flame,* vol. 188, pp. 488-497, 2018.
[17] X. Liu, J. Jeffries, R. Hanson, K. Hinckley, and M. Woodmansee, "Development of a tunable diode laser sensor for measurements of gas turbine exhaust temperature," *Applied Physics B,* vol. 82, pp. 469-478, 2006.
[18] I. A. Schultz, C. S. Goldenstein, J. B. Jeffries, R. K. Hanson, R. D. Rockwell, and C. P. Goyne, "Spatially-resolved TDLAS measurements of temperature, H2O column density, and velocity in a direct-connect scramjet combustor," in *52nd Aerospace Sciences Meeting*, 2014, p. 1241.
[19] A. Upadhyay *et al.*, "Tomographic imaging of carbon dioxide in the exhaust plume of largecommercial aero-engines," *Applied Optics,* vol. 61, no. 28, pp. 8540-8552, 2022, doi: 10.1364/AO.467828.
[20] A. L. Chakraborty, K. Ruxton, and W. Johnstone, "Suppression of intensity modulation contributions to signals in second harmonic wavelength modulation spectroscopy," *Optics letters,* vol. 35, no. 14, pp. 2400-2402, 2010.
[21] C. S. Goldenstein, R. M. Spearrin, J. B. Jeffries, and R. K. Hanson, "Infrared laser-absorption sensing for combustion gases," *Progress in Energy and Combustion Science,* vol. 60, pp. 132-176, 2017.
[22] Z. Du, Y. Yan, J. Li, S. Zhang, X. Yang, and Y. Xiao, "In situ, multiparameter optical sensor for monitoring the selective catalytic reduction process of diesel engines," *Sensors and Actuators B: Chemical,* vol. 267, pp. 255-264, 2018.
[23] K. Duan, Y. Ji, D. Wen, Z. Lu, K. Xu, and W. Ren, "Mid-infrared fiber-coupled laser absorption sensor for simultaneous NH3 and NO monitoring in flue gases," *Sensors and Actuators B: Chemical,* vol. 374, p. 132805, 2023.
[24] C. S. Goldenstein, C. L. Strand, I. A. Schultz, K. Sun, J. B. Jeffries, and R. K. Hanson, "Fitting of calibration-free scanned-wavelength-modulation spectroscopy spectra for determination of gas properties and absorption lineshapes," *Applied optics,* vol. 53, no. 3, pp. 356-367, 2014.
[25] A. Klein, O. Witzel, and V. Ebert, "Rapid, time-division multiplexed, direct absorption-and wavelength modulation-spectroscopy," *Sensors,* vol. 14, no. 11, pp. 21497-21513, 2014.
[26] I. E. Gordon *et al.*, "The HITRAN2016 molecular spectroscopic database," *Journal of Quantitative Spectroscopy and Radiative Transfer,* vol. 203, pp. 3-69, 2017.
[27] Y. Bao *et al.*, "Relative entropy regularized TDLAS tomography for robust temperature imaging," *IEEE Transactions on Instrumentation and Measurement,* vol. 70, pp. 1-9, 2020.
[28] A. Huang, Z. Cao, W. Zhao, H. Zhang, and L. Xu, "Frequency-division multiplexing and main peak scanning WMS method for TDLAS tomography in flame monitoring," *IEEE Transactions on Instrumentation and Measurement,* vol. 69, no. 11, pp. 9087-9096, 2020.
[29] R. S. Tucker, G. Eisenstein, and S. K. Korotky, "Optical time-division multiplexing for very high bit-rate transmission," *Journal of lightwave technology,* vol. 6, no. 11, pp. 1737-1749, 1988.
[30] N. Liu, L. Xu, S. Zhou, L. Zhang, and J. Li, "Simultaneous detection of multiple atmospheric components using an NIR and MIR laser hybrid gas sensing system," *ACS sensors,* vol. 5, no. 11, pp. 3607-3616, 2020.
[31] L. Xu, S. Zhou, N. Liu, M. Zhang, J. Liang, and J. Li, "Multigas sensing technique based on quartz crystal tuning fork-enhanced laser spectroscopy," *Analytical Chemistry,* vol. 92, no. 20, pp. 14153-14163, 2020.
[32] G. Enemali, R. Zhang, H. McCann, and C. Liu, "Cost-effective quasi-parallel sensing instrumentation for industrial chemical species tomography," *IEEE Transactions on Industrial Electronics,* vol. 69, no. 2, pp. 2107-2116, 2021.
[33] N. A. Malarich and G. B. Rieker, "Resolving nonuniform temperature distributions with single-beam absorption spectroscopy. Part I: Theoretical capabilities and limitations," *Journal of Quantitative Spectroscopy and Radiative Transfer,* vol. 260, p. 107455, 2021.

Rui Zhang received the B.Eng. degree (Hons.) in electronics and electrical engineering with management from University of Edinburgh, U.K., in 2019. She is currently pursuing a Ph.D. degree in School of Engineering, University of Edinburgh. Her current research interest is focused on laser absorpGon spectroscopic sensor design for combusGon diagnosis.
Jiangnan Xia received the B.Eng. degree (Hons.) in electrical and electronics engineering from University of Edinburgh, U.K., in 2020. He is currently pursuing a Ph.D. degree in the School of Engineering, University of Edinburgh. His current research interests are embedded system design for laser sensing and imaging.
Ihab Ahmed is working as a research associate at the University of Sheffield, where he is currently pursuing a Ph.D. degree in Future Gas Turbine CombusGon. Ihab has gained extensive experience in studying the effects of alternaGve fuels on combusGon and emissions. His research interests also encompass combustor design, fuel delivery systems and combusGon dynamics.
Ian Armstrong received the B.Eng. (First Class Hons.) degree in electronic and electrical engineering from the University of Strathclyde, Glasgow, U.K., in 2001, and the Eng.D. degree from the University of Strathclyde in 2006. He is working as a Research Fellow at the Centre for Microsystems and Photonics, University of Strathclyde, developing TDLS-based gas detecGon systems in the near- and mid-IR spectral regions.
Abhishek Upadhyay received Ph.D. degree from Indian InsGtute of Technology, Gandhinagar in January 2017. From February 2017 to August 2022, he was a post-doctoral researcher at the University of Strathclyde, Glasgow. From September 2022, he has been a post-doctoral researcher at the University of Edinburgh. His current research interests include image reconstrucGon for combusGon diagnosGcs.
Yalei Fu received the B.Eng. degree (Hons.) in electronic and electrical engineering from University of Edinburgh, U.K., in 2020. She is currently pursuing a Ph.D. degree in the School of Engineering, University of Edinburgh. Her research interests are focusing on deep learning aided laser spectroscopic sensing and imaging.
Godwin Enemali received Ph.D. degrees in electronics engineering from The University of Edinburgh, Edinburgh, U.K., in 2019. From 2018 to April 2022, he was a Research Associate in the School of Engineering, University of Edinburgh. Since April 2022, he has been a lecturer in the department of Electrical and Electronic Engineering at Glasgow Caledonian University.
Michael Lengden joined the Centre for Microsystems and Photonics in the EEE department at the University of Strathclyde, Glasgow, U.K. as a Research Fellow, and is now a Reader in the same department. He is engaged in research into high-temperature and high-pressure gas composiGon measurements using tunable diode laser spectroscopy for harsh environments, such as aero-engine exhausts, mid-pressure liquid fuel combusGon rigs, and solid oxide fuel cells.
Walter Johnstone is the Research Professor of Photonic Systems in the Department of Electronic and Electrical Engineering (EEE) at the University of Strathclyde. He is responsible for leading research in the field of applied laser spectroscopy for gas measurements in extreme environments, such as gas turbine aero-engines. Prior to his current posiGon, he held senior management posts as Deputy Head then Head of Electronic and Electrical Engineering (2006-11) and Vice Dean (Research) of the Faculty of Engineering (2001-16).
Krikor B. Ozanyan received the M.Sc. degree in engineering physics (semiconductors) and the Ph.D. degree in solid-state physics in 1980 and 1989, respecGvely. He is currently the Director of Research with the Department of EEE, The University of Manchester, U.K. He has more than 300 publicaGons in the areas of photonic materials, devices, and systems for sensing and imaging. He is a Fellow of the InsGtute of Engineering and Technology, U.K., and the InsGtute of Physics, U.K. He was the Editor-in-Chief of the IEEE Sensors Journal from 2011 to 2018 and the General Co-Chair of the IEEE SENSORS 2017 Conference. He serves as the Vice-President for publicaGons of the IEEE Sensors Council.
Mohamed Pourkashanian is the managing director of the TranslaGonal Energy Research Centre and head of Energy2050 and energy research at The University of Sheffield. He has completed numerous major research projects on CCUS clean energy technology and received substanGal grants from the EPSRC, EU, NATO and industry. He has published over 400 refereed research papers and is a member of numerous internaGonal and naGonal scienGfic bodies.

Hugh McCann is Professor of Tomographic Imaging at The University of Edinburgh, U.K., where he was Head of the School of Engineering (2013-18). He was Professor of Industrial Tomography (1996-2013) at the University of Manchester, Manchester, U.K., following ten years in R&D at the Royal Dutch/Shell Group. He has extended industrial tomography to provide specific chemical contrast using high-speed all-opto-electronic techniques, and has developed electrical impedance tomography for medical applicaGons. He was the Head of the School of Electrical and Electronic Engineering at Manchester (1999-2002), and Chair of the U.K. Professors and Heads of Electrical Engineering (2003-05). Prof. McCann was elected a Fellow of the Royal Academy of Engineering in 2009 and a Fellow of the Royal Society of Edinburgh in 2015. In 2018 he was appointed Honorary Professor at Beihang University, Beijing, China.
Chang Liu received the Ph.D. degree in tesGng, measurement technology, and instrument from Beihang University, China, in 2016. From April 2016 to January 2018, he was a Post-Doctoral Researcher with the Department of Air PolluGon and Environmental Technology, Empa, Switzerland. Since February 2018, he has been a Lecturer with the School of Engineering, University of Edinburgh, U.K. His current research interests include laser absorpGon spectroscopy, acGve/passive opGcal tomography techniques and system design, and their applicaGons to combusGon diagnosis and environmental monitoring.

Rui Zhang performed experiments, result analysis and originally drafted the paper. **Jiangnan Xia**, **Andrew Gough** and **Godwin Enemali** performed hardware design and experiments. **Ihab Ahmed** and **Ian Armstrong** performed experiments and results analysis. **Abhishek Upadhyay** and **Yalei Fu** performed signal processing. **Michael Lengden, Walter Johnstone, Paul Wright, Krikor Ozanyan, Mohamed Pourkashanian** and **Hugh McCann** performed reviewing and editing of the paper. **Chang Liu** conceptualized the paper, supervised the experiments and results analysis, and performed reviewing and editing.

Declaration of interests

☐ The authors declare that they have no known competing financial interests or personal relationships that could have appeared to influence the work reported in this paper.

☒ The authors declare the following financial interests/personal relationships which may be considered as potential competing interests:

Chang Liu reports financial support was provided by Engineering and Physical Sciences Research Council.

Highlights
• A fast TDLAS sensor is developed to measure H2O and temperature in turbine exhaust.
• The developed sensor is validated via in situ tests on a commercial gas turbine.
• Edge effect is quantified in real time to enable accurate plume measurement.
• The sensor reveals underlying engine combustion dynamics and control behaviors.